IEEE Photonics Journal
An IEEE Photonics Society Publication

Residual Intensity Modulation Induced Error in Resonator Fiber Optic Gyroscopes With Reciprocal Detection

Volume 13, Number 3, June 2021

Zhiguo Jiang
Ruqing Chen
Zongfu Hu

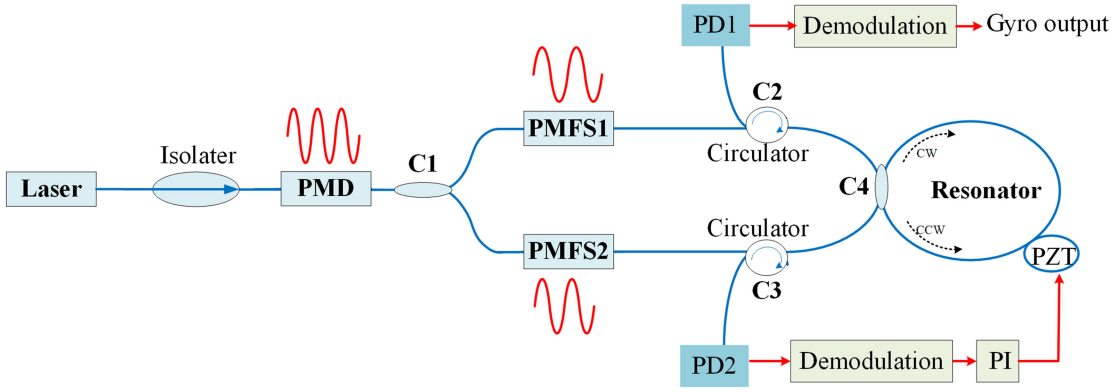

DOI: 10.1109/JPHOT.2021.3081584

Residual Intensity Modulation Induced Error in Resonator Fiber Optic Gyroscopes With Reciprocal Detection

Zhiguo Jiang ,[1] Ruqing Chen,[1] and Zongfu Hu[2]

[1]College of Information Science and Engineering, Jiaxing University, Jiaxing 314001, China
[2]College of Electronics and Information Engineering, Tongji University, Shanghai 201806, China

DOI:10.1109/JPHOT.2021.3081584

Manuscript received April 19, 2021; revised May 12, 2021; accepted May 16, 2021. Date of publication May 18, 2021; date of current version May 31, 2021. This work was supported by the scientific research start-up fund of Jiaxing University under Grant CD70520028. Corresponding author: Zhiguo Jiang (e-mail: xidianzhiguo@163.com).

Abstract: In the resonator fiber optic gyroscope (RFOG), both the residual intensity modulation (RIM)-induced error and backscattering-induced noise need to be effectively suppressed. When the clockwise and counterclockwise resonance detection adopt the same phase modulation and demodulation scheme, namely reciprocal detection, the reciprocity of the RFOG is improved, and the error induced by the RIM of the phase modulator used for detection (PMD) can be effectively suppressed. However, it is inevitable to add a phase modulator used for frequency shift (PMFS) to suppress the backscattering-induced noise. In this paper, the influence of the RIM of the PMFS on the performance of the RFOG is analyzed, and the model of the RIM-induced error in the RFOG with reciprocal detection is established. The analysis shows that in order to reduce the bias to the level of the shot noise, it is necessary to suppress the error induced by the RIM of the PMFS, and reducing the modulation frequency of the PMFS can effectively suppress the RIM-induced error. When a phase modulator is added to the RFOG with reciprocal detection to further suppress the backscattering-induced noise, the RIM-induced error can still be effectively suppressed by reducing the frequency of the added phase modulation.

Index Terms: Resonator fiber optic gyroscope, residual intensity modulation, phase modulation, backscattering induced noise.

1. Introduction

The resonator fiber optic gyroscope (RFOG) obtains the angular velocity by measuring the resonance center frequency shift between the clockwise (CW) and counterclockwise (CCW) directions in a fiber ring resonator (FRR) [1]. The RFOG development efforts are motivated by the theoretical potential to meet navigation grade performance in a smaller size and lower cost than the ring laser gyro (RLG) and the interferometric fiber optic gyroscope (IFOG) [2]. This is due to the fact that the RFOG combines sensitivity-increasing signal to noise attributes of recirculating the light in a resonant cavity like an RLG, concomitant with the ability to wind longer path-length multi-turn coils like an IFOG, using optical fiber [3].

The error mechanisms drive the design improvement of the RFOG [4]–[7]. However, the error induced by the residual intensity modulation (RIM) of the electro-optical phase modulator (EOPM) and the backscattering-induced noise have typically driven designs in different directions [3]. The

suppression of the backscattering-induced noise requires that the frequencies of CW and CCW phase modulation are different to reduce the same frequency components of the CW and CCW light waves [8],[9],[10]. However, the suppression of the RIM-induced error expects that the phase modulation-demodulation scheme is the same for the CW and CCW resonance detection [4],[11]. One requires different phase modulations in the CW and CCW directions, and the other requires the same phase modulation in the CW and CCW directions. Compared with the RIM-induced error, the backscattering-induced noise have a greater impact on the RFOG performance. Therefore, the backscattering-induced noise is the main concern [12],[13]. However, as the precision of the RFOG continues to improve, approaching the inertial navigation grade, the RIM-induced error has gradually attracted attention [3],[4],[14]. Both the RIM-induced error and the backscattering-induced noise need to be effectively suppressed.

In the RFOG, the RIM of the phase modulator leads to a nonzero output signal at the resonance center frequency [15]. Zhang et al. used the output of the phase modulator to compensate for the deviation of the resonance center frequency detection caused by the RIM [16]. Sanders et al. proposed an improved modulation technique in a three-laser RFOG configuration to reduce the drift due to optical backscatter while retaining a common modulation for CW and CCW resonance detection to eliminate the RIM-induced error [3]. Jiang et al. established the model of the RIM-induced error in the RFOG with triangular phase modulation [14], and demonstrated an improved modulation scheme to suppress the backscattering-induced noise while reducing the RIM-induced error [11]. Ma et al. theoretically analyzed the RIM-induced error in the RFOG with sinusoidal wave phase modulation [15], and proposed the RFOG using reciprocal detection [4], where the CW and CCW resonance detection are realized by the same phase modulation and demodulation, and the backscattering induced noise is suppressed by adding other phase modulators for frequency shift (PMFS). In Ref.4, the analysis shows that the error induced by the RIM of the phase modulator used for resonance detection (PMD) can be effectively suppressed in the RFOG with reciprocal detection. However, the influence of the RIM of the PMFS on the performance of the RFOG with reciprocal detection has not been analyzed.

In this paper, we established the model of the RIM-induced error in the RFOG with reciprocal detection, and analyzed the influences of the RIM depth, the modulation frequency of the phase modulator used for frequency shift (PMFS), and double phase modulation technique on the RIM-induced error in the RFOG with reciprocal detection.

2. Model of RIM-induced Error in the RFOG with Reciprocal Detection

The RIM in the EOPM is not the result of a single physical mechanism but due to the combined effects of environmental, beam, and medium properties [17]. Karl Kissa et al. pointed out that the phase modulation creates the RIM due to several effects with the chip. First, (a) the electric field from the electrodes modifies the refractive index profile within the waveguide slightly, causing the mode shape to change slightly, and the voltage-dependent optical loss creates intensity modulation that is nearly linear with applied voltage [18]. Second, (b) a portion of the light radiated within the substrate is reflected with the substrate, and the coherent interference of the main beam with the stray light component creates intensity modulation [18]. The first effect can be classified as linear RIM, and the second effect can be classified as non-linear RIM.

The IFOG uses a wide linewidth light source, and the RFOG uses a narrow linewidth light source. In the IFOG, Lefevre pointed out that the coherent interference of the transmitted TE wave with the TE stray wave creates a typical power variation of $\pm 2 \times 10^{-4}$[1]. Because of the wide linewidth and the strong birefringence of the $LiNbO_3$ phase modulator, depolarization is very fast and the interference of the TM wave with the TE wave does not create intensity modulation. However, the RFOG uses a narrow linewidth light source, so the strong birefringence of the $LiNbO_3$ phase modulator cannot depolarize the light incident on the phase modulator. Therefore, in addition to the above (a) and (b), the coherent interference of the TM wave with the TE wave will create intensity modulation in the RFOG. The RIM generated by this mechanism can be classified into non-linear RIM.

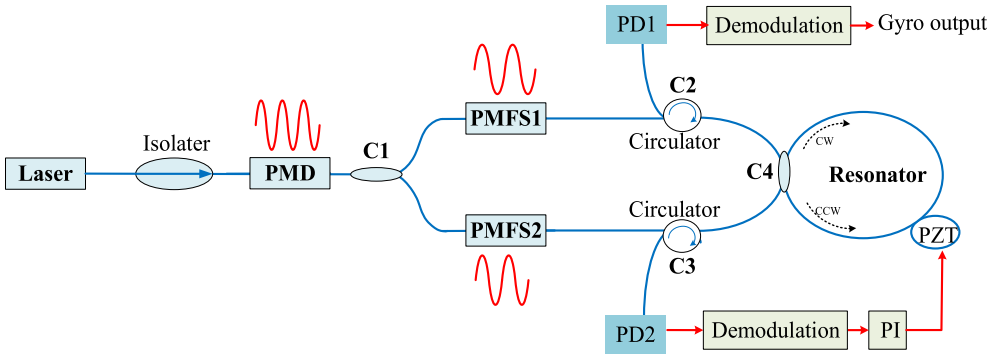

Fig. 1. Schematic diagram of the RFOG with reciprocal detection.

The schematic diagram of the RFOG with reciprocal detection is shown in Fig. 1. All the fibers and couplers are polarization maintaining operation. The center wavelength and the linewidth of the light source is 1550nm and 4.5KHz, respectively. The laser passes through the phase modulator PMD, and then is divided into two waves by the 3dB coupler C1. The two waves are phase modulated by the phase modulators PMFS1 and PMFS2 respectively, and then are launched into the FRR through the coupler C4 to form the CW and CCW waves. After the CW and CCW waves leave the FRR, they are coupled to photodetectors PD1 and PD2 by circulators C2 and C3, respectively. In the FRR, a segment fiber is tightly wound around the PZT cylinder, and the cavity length can be adjusted by the voltage on the PZT. The CCW path is the reference path, which is used to lock the resonance center frequency of the CCW direction at the laser frequency. The CW path is the signal path, which is used to obtain the output signal of the RFOG. The modulation frequency and modulation index of the PMD are f_D and M_D, respectively. The modulation frequency and modulation index of the PMFS1 are f_1 and M_1, respectively. The modulation frequency and modulation index of the PMFS2 are f_2 and M_2, respectively.

The incident light field of the phase modulator can be written as

$$E(t) = E_0 e^{-i2\pi f_s t} \tag{1}$$

where E_0 is the amplitude of the electric field of the light source, and f_S is the frequency of the light source. The phase of the light wave is modulated by the phase modulator with the signal $V(t) = V_0 \sin 2\pi f_0 t$. Nevertheless, the intensity modulation will also be induced, and the output intensity of the phase modulator can be expressed as

$$I(t) = |E_0|^2 (1 + R(t)) \tag{2}$$

where $R(t) \approx \chi \cdot V_0 \sin 2\pi f_0 t$ represents the RIM and is a function of $\sin 2\pi f_0 t$, and $\varepsilon \approx \chi \cdot V_0$ is the modulation depth of the RIM.

The reciprocal detection of the RFOG is that the CW and CCW resonance detection is realized by the same phase modulation-demodulation. In Fig. 1, the phase modulator PMD is designed for the CW and CCW resonance detection in the RFOG, where the error induced by the RIM of the PMD can be effectively suppressed [4],[11]. The phase modulators PMFS1 and PMFS2 are designed for frequency shift in the CCW and CW directions respectively to suppress the backscattering-induced noise, and the RIM depth of the PMFS1 and PMFS2 are ε_1 and ε_2, respectively. In the RFOG with reciprocal detection, the frequency of the phase modulation and demodulation used for the CW and CCW resonance detection is f_D, which is different from the modulation frequency of the PMFS1 or PMFS2. Therefore, in the frequency domain, only the DC component of the light wave modulated by the PMFS1 or PMFS2 and passing through the FRR will affect the output of the synchronous demodulation.

Next, the DC component just mentioned is analyzed, and the DC component related to the RIM of the PMFS is derived.

2.1 DC Component of the Light Wave Passing Through the FRR

Taking the PMFS1 as an example, the influence of the PMD on the DC component is ignored, and the output electric field of the PMFS1 can be written as

$$E(t)=\frac{\sqrt{2}}{2}\left(1+\frac{1}{2}\varepsilon_1\sin(2\pi f_1 t)\right)E_0 e^{-i(2\pi f_s t+M_1\sin(2\pi f_1 t))} \tag{3}$$

Using the Bessel function expansion and the overlapping field methods, the output electric field of the FRR can be written as

$$E(t)=\frac{\sqrt{2}}{2}\left(1+\frac{1}{2}\varepsilon_1\sin(2\pi f_1 t)\right)E_0\sum_{m=-\infty}^{\infty}J_m(M_1)e^{-i(2\pi f_s t+2\pi m f_1 t)}h_m e^{i\phi_m} \tag{4}$$

$$h_m=\sqrt{(1-\gamma)\left(1-\frac{K\gamma}{(1-R)^2+4R\sin^2(\pi\cdot\tau\cdot(mf_1+\Delta f))}\right)} \tag{5}$$

$$\phi_m=\arctan\frac{K\sqrt{1-\gamma}\sin(2\pi\cdot\tau\cdot(mf_1+\Delta f))}{(2-\gamma)\sqrt{1-K}-(2-K)\sqrt{1-\gamma}\cos(2\pi\cdot\tau\cdot(mf_1+\Delta f))} \tag{6}$$

where h_m and ϕ_m are the amplitude and phase transfer functions of the FRR respectively, Δf is frequency deviation between the laser frequency and the resonance center frequency, $R=\sqrt{(1-K)(1-\gamma)}$, K and γ are the coupling coefficient and insertion loss of the coupler C4 respectively, $\tau=n_e L/c$ is the traveling time in the FRR, L is the cavity length, n_e is the refractive index of the fiber, and c is the speed of light.

The output voltage of the PD2 can be derived as

$$V(t)=\frac{1}{2}R_e(1+\varepsilon_1\sin(2\pi f_1 t))E_0^2\sum_{m=-\infty}^{\infty}\sum_{m'=-\infty}^{\infty}\left(J_m(M_1)J_{m'}(M_1)e^{i(2\pi(m-m')f_1 t)}h_m h_{m'}e^{i(\phi_m-\phi_{m'})}\right) \tag{7}$$

where R_e is the response factor of the PD1 and PD2.

Therefore, the DC component of the light wave modulated by the PMFS1 and passing through the FRR can be derived as

$$V_{DC}=\frac{1}{2}R_e E_0^2\sum_{m=-\infty}^{\infty}\left(J_m^2(M_1)h_m^2-\varepsilon_1 J_{m+1}(M_1)J_m(M_1)h_{m+1}h_m\sin(\phi_{m+1}-\phi_m)\right) \tag{8}$$

According to Eq.8, the DC component will be affected by the RIM of the PMFS. The DC component related to the RIM can be expressed as

$$V_{DC-RIM}=-\frac{1}{2}\varepsilon_1 R_e E_0^2\sum_{m=-\infty}^{\infty}\left(J_{m+1}(M_1)J_m(M_1)h_{m+1}h_m\sin(\phi_{m+1}-\phi_m)\right) \tag{9}$$

There is a difference between the RIM depth of the PMFS1 and PMFS2, and the difference will change with time. Therefore, the DC component related to the RIM of the PMFS are different in the CW and CCW directions, so the difference in the RIM between the PMFS1 and PMFS2 will destroy the reciprocity between the CW and CCW directions, and the RIM of the PMFS will affect the zero drift of the RFOG.

Fig. 2 depicts the relationship between V_{DC-RIM}, modulation frequency f_1, and working point frequency Δf, where $R_e E_0^2=2$, $\varepsilon_1=0.001$. In Fig. 2, no matter where the work point is located, with the decrease of the modulation frequency f_1, the absolute value of V_{DC-RIM} will also decrease, which implies that the RIM-induced error can be suppressed by reducing the modulation frequency of the PMFS.

Next, we establish the model of the RIM-induced error in the RFOG with reciprocal detection, and analyze the influence of the RIM of the PMFS on the performance of the RFOG.

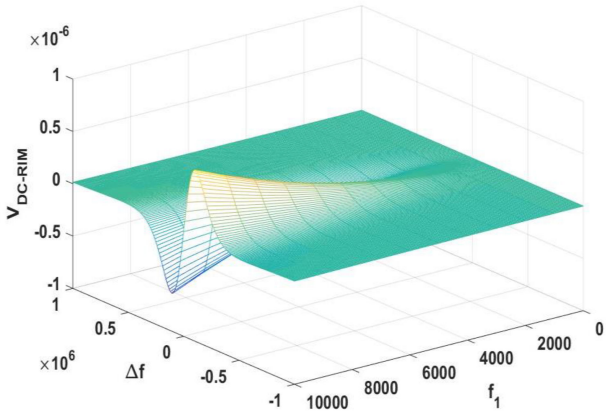

Fig. 2. Relationship between V_{DC-RIM}, f_1 and Δf.

2.2 RIM-induced Error in the RFOG with Reciprocal Detection

In the RFOG with reciprocal detection, the laser passes through the phase modulator PMD, and the output electric field of the PMD can be written as

$$E(t) = E_0 e^{-i(2\pi f_s t + M_D \sin(2\pi f_D t))} \tag{10}$$

where the RIM of the PMD is ignored, because the RIM of the PMD is reciprocal between the CW and CCW directions.

Taking the CW path as an example, and the output electric field of the PMFS2 can be written as

$$E(t) = \frac{\sqrt{2}}{2}\left(1+\frac{1}{2}\varepsilon_2 \sin(2\pi f_2 t)\right) E_0 e^{-i(2\pi f_s t + M_D \sin(2\pi f_D t) + M_2 \sin(2\pi f_2 t))} \tag{11}$$

Using the Bessel function expansion and the overlapping field methods, the output electric field of the FRR can be written as

$$E_{cw}(t) = \frac{\sqrt{2}}{2}\left(1+\frac{1}{2}\varepsilon_2 \sin(2\pi f_2 t)\right) E_0 \sum_{n=-\infty}^{\infty}\sum_{m=-\infty}^{\infty} J_n(M_D) J_m(M_2) e^{-i(2\pi f_s t + 2\pi n f_D t + 2\pi m f_2 t)} h_{(n,m)} e^{i\phi_{(n,m)}} \tag{12}$$

$$h_{(n,m)} = \sqrt{(1-\gamma)\left(1 - \frac{K\gamma}{(1-R)^2 + 4R\sin^2(\pi \cdot \tau \cdot (nf_D + mf_2 + \Delta f))}\right)} \tag{13}$$

$$\phi_{(n,m)} = \arctan \frac{K\sqrt{1-\gamma}\sin(2\pi \cdot \tau \cdot (nf_D + mf_2 + \Delta f))}{(2-\gamma)\sqrt{1-K} - (2-K)\sqrt{1-\gamma}\cos(2\pi \cdot \tau \cdot (nf_D + mf_2 + \Delta f))} \tag{14}$$

where $h_{(n,m)}$ and $\phi_{(n,m)}$ are the amplitude and phase transfer functions of the FRR respectively.

The output voltage of the PD1 can be derived as

$$\begin{aligned} V(t) = {} & \frac{1}{2} R_e (1+\varepsilon_2 \sin(2\pi f_2 t)) E_0^2 \sum_{n=-\infty}^{\infty}\sum_{m=-\infty}^{\infty}\sum_{n'=-\infty}^{\infty}\sum_{m'=-\infty}^{\infty} \\ & \times \begin{pmatrix} J_n(M_D) J_m(M_2) J_{n'}(M_D) J_{m'}(M_2) \\ \times e^{i(2\pi(n-n')f_D t + 2\pi(m-m')f_2 t)} h_{(n,m)} h_{(n',m')} e^{i\left(\phi_{(n,m)} - \phi_{(n',m')}\right)} \end{pmatrix} \end{aligned} \tag{15}$$

TABLE I
Parameters of the RFOG

Diameter D of the FRR	0.06 m
Cavity length L of the FRR	10 m
Coupling coefficient K of the C4	0.03
Insertion loss γ of the C4	0.12
Input light intensity of the FRR	1mW
Noise equivalent power P_s of the PD1	10pW
Noise equivalent power P_s of the PD2	10pW
Modulation index M_D, M_1, M_2	2.405

The frequency spectrum at f_D derived from Eq. 15 can be expressed as

$$V_{f_D} = R_e E_0^2 \sum_{n=-\infty}^{\infty} \sum_{m=-\infty}^{\infty} \left(J_n(M_D) J_{n+1}(M_D) J_m^2(M_2) h_{(n,m)} h_{(n+1,m)} \cos\left(2\pi f_D t + \phi_{(n,m)} - \phi_{(n+1,m)}\right)\right)$$
$$+\varepsilon_2 R_e E_0^2 \sin(2\pi f_2 t) \sum_{n=-\infty}^{\infty} \sum_{m=-\infty}^{\infty} \left(\begin{array}{l} J_n(M_D) J_{n+1}(M_D) J_{m+1}(M_2) J_m(M_2) \times \\ \left(\begin{array}{l} h_{(n+1,m+1)} h_{(n,m)} \cos\left(2\pi f_D t + 2\pi f_2 t + \phi_{(n+1,m+1)} - \phi_{(n,m)}\right) + \\ h_{(n+1,m)} h_{(n,m+1)} \cos\left(2\pi f_D t - 2\pi f_2 t + \phi_{(n+1,m)} - \phi_{(n,m+1)}\right) \end{array} \right) \end{array} \right) \tag{16}$$

It can be seen that the signal of frequency f_D can be generated by mixing the RIM of frequency f_2 and the signal of frequency $f_D + f_2$ or the signal of frequency $f_D + f_2$.

The voltage component at frequency f_D are demodulated by the lock-in amplifier (LIA). The demodulated signal from the LIA can be expressed as

$$\Delta V(\Delta f) = \frac{1}{2} R_e E_0^2 \sum_{n=-\infty}^{\infty} \sum_{m=-\infty}^{\infty} \left(J_n(M_D) J_{n+1}(M_D) J_m^2(M_2) h_{(n,m)} h_{(n+1,m)} \sin\left(\phi_{(n+1,m)} - \phi_{(n,m)}\right)\right)$$
$$-\frac{1}{4} \varepsilon_2 R_e E_0^2 \sum_{n=-\infty}^{\infty} \sum_{m=-\infty}^{\infty} \left(\begin{array}{l} J_n(M_D) J_{n+1}(M_D) J_{m+1}(M_2) J_m(M_2) \times \\ \left(h_{(n+1,m+1)} h_{(n,m)} \cos\left(\phi_{(n+1,m+1)} - \phi_{(n,m)}\right) - h_{(n+1,m)} h_{(n,m+1)} \cos\left(\phi_{(n+1,m)} - \phi_{(n,m+1)}\right)\right) \end{array} \right) \tag{17}$$

where the first term is the output signal of the RFOG, and the second term is the error induced by the RIM of the PMFS2. Therefore, the RIM-induced error in the RFOG with reciprocal detection can be expressed as

$$\Delta V_{error}(\Delta f) = -\frac{1}{4} \varepsilon_2 R_e E_0^2 \sum_{n=-\infty}^{\infty} \sum_{m=-\infty}^{\infty} \left(\begin{array}{l} J_n(M_D) J_{n+1}(M_D) J_{m+1}(M_2) J_m(M_2) \times \\ \left(\begin{array}{l} h_{(n+1,m+1)} h_{(n,m)} \cos\left(\phi_{(n+1,m+1)} - \phi_{(n,m)}\right) - \\ h_{(n+1,m)} h_{(n,m+1)} \cos\left(\phi_{(n+1,m)} - \phi_{(n,m+1)}\right) \end{array} \right) \end{array} \right) \tag{18}$$

3. Analysis of the RIM-induced Error

Before the analysis of the RIM-induced error, we first calculate the sensitivity of the RFOG. In Fig. 1, the parameters of the RFOG are shown in Table I.

The RFOG sensitivity limited by the shot noise of the detectors can be expressed as

$$\Omega_s = \frac{n_e \lambda}{D} \frac{\Delta f_{FWHM}}{P_{max} - P_{min}} \frac{\sqrt{2} P_s}{2} = \frac{\sqrt{2} P_s}{P_{max} - P_{min}} \frac{\lambda c}{2 \cdot L \cdot D \cdot F} \tag{19}$$

where P_{max} and P_{min} are the maximum and minimum power of the resonance curve, respectively. After calculation, the free spectral range (FSR) is approximately 20MHz, and the finesse F of the FRR is 40, and the full width at half maximum (FWHM) of the resonance Δf_{FWHM} is approximately 500kHz, and the sensitivity is approximately 0.05°/h.

Next, we analyze the influences of the RIM depth ε_2, the frequencies f_D and f_2, and the double phase modulation technique on the error induced by the RIM of the PMFS in the RFOG. In the following simulation, $R_e E_0^2$ is set to 50V, which is determined by the LIA.

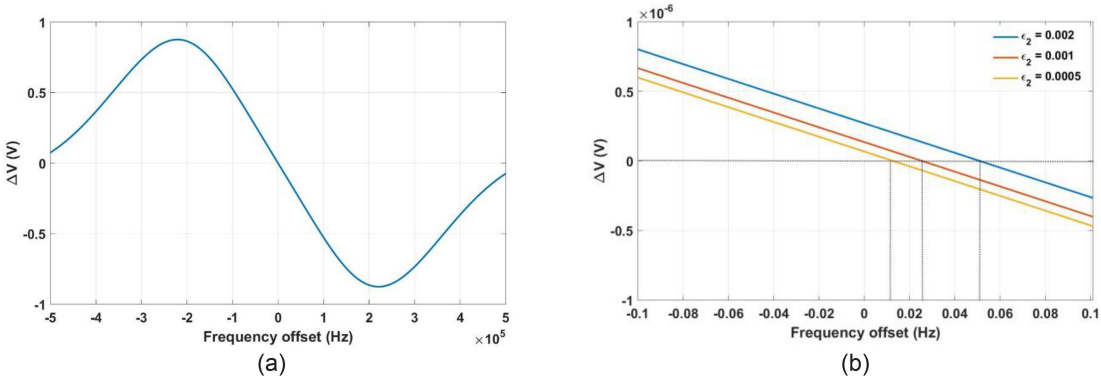

Fig. 3. (a) Demodulation curve (b) Demodulation curve at origin.

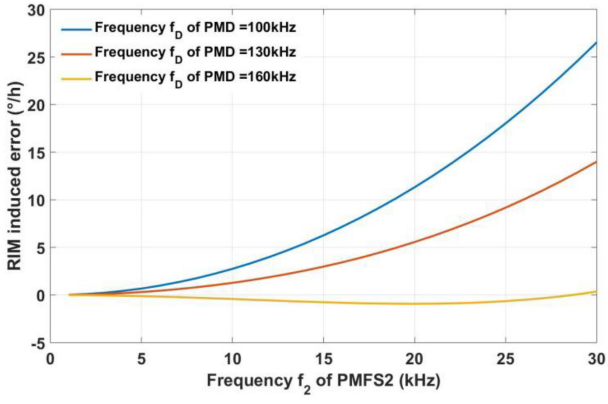

Fig. 4. Relationship between f_D, f_2 and RIM-induced error.

3.1 RIM Depth

Generally, the RIM depth $\varepsilon \approx \chi \cdot V_0$ increases as the amplitude V_0 of modulation signal increases. When V_0 equals to V_π, the RIM depth ε of the phase modulator is about $0.0001 \sim 0.002$. The maximum slope point of the resonance curve is 130kHz away from the resonance center frequency. According to Eq. 18, Fig. 3(a) depicts the demodulation curve of the RFOG, and Fig. 3(b) depict the demodulation curves of the RFOG with different RIM depths ε_2, where f_D=130kHz and f_2= 4kHz. In Fig. 3(b), it can be seen that the demodulation output at the resonance center frequency no longer corresponds to the zero point, and there is an offset error. When the RIM depths are 0.002, 0.001 and 0.0005 respectively, the zero-offset error are 0.05Hz, 0.025Hz and 0.0125Hz respectively, which correspond to a gyro bias of 0.4°/h, 0.2°/h and 0.1°/h respectively. The results show that in order to reduce the bias to the level of the shot noise, it is necessary to suppress the error induced by the RIM of the PMFS.

3.2 Frequencies of PMD and PMFS

The frequencies of the PMD and the PMFS are the key parameters of the RFOG. According to Eq. 18, Fig. 4 depicts the relationship between f_D, f_2 and the RIM-induced error, where $\varepsilon_2 = 0.001$. It can be seen that when f_D is 100kHz or 130kHz, the RIM-induced error decreases as f_2 decreases. Therefore, the error induced by the RIM of the PMFS can be suppressed by reducing the frequency of the PMFS. Taking $f_2 = 1$kHz as an example, when f_D are 100kHz, 130 kHz and 160 kHz, the RIM-induced error are 0.023°/h, 0.015°/h and -0.008°/h respectively, which are all less than the sensitivity of the RFOG.

In Fig. 4, we notice that when f_D and f_2 are 160kHz and 28.625kHz respectively, the RIM-induced error is approximately zero. Actually, the RIM signal of the PMFS2 with frequency f_2 influences the CW resonance detection by mixing with the signals at frequency $f_D - f_2$ and $f_D + f_2$. The signals at frequency $f_D - f_2$ and $f_D + f_2$ on the PD1 can be derived as

$$V_{f_D-f_2} = R_e E_0^2 \sum_{n=-\infty}^{\infty} \sum_{m=-\infty}^{\infty} \left(J_n(M_D) J_{n+1}(M_D) J_{m+1}(M_2) J_m(M_2) h_{(n+1,m)} h_{(n,m+1)} \right. \\ \left. \times \cos\left(2\pi f_D t - 2\pi f_2 t + \phi_{(n+1,m)} - \phi_{(n,m+1)}\right)\right) \tag{20}$$

$$V_{f_D+f_2} = R_e E_0^2 \sum_{n=-\infty}^{\infty} \sum_{m=-\infty}^{\infty} \left(J_n(M_D) J_{n+1}(M_D) J_{m+1}(M_2) J_m(M_2) h_{(n+1,m+1)} h_{(n,m)} \right. \\ \left. \times \cos\left(2\pi f_D t + 2\pi f_2 t + \phi_{(n+1,m+1)} - \phi_{(n,m)}\right)\right) \tag{21}$$

It can be seen that the amplitude changes of the signals at frequency $f_D - f_2$ and $f_D + f_2$ are different after passing through the resonator, and the phase changes of the signals at frequency $f_D - f_2$ and $f_D + f_2$ are also different. The RIM signal at frequency f_2 will be mixed with the signals at frequency $f_D - f_2$ and $f_D + f_2$ respectively, and the two mixed signals at frequency f_D can be derived as

$$V_{f_2\times(f_D-f_2)} = \frac{1}{2}\varepsilon_2 R_e E_0^2 \sum_{n=-\infty}^{\infty} \sum_{m=-\infty}^{\infty} \\ \times \left(J_n(M_D) J_{n+1}(M_D) J_{m+1}(M_2) J_m(M_2) h_{(n+1,m)} h_{(n,m+1)} \sin\left(2\pi f_D t + \phi_{(n+1,m)} - \phi_{(n,m+1)}\right)\right) \tag{22}$$

$$V_{f_2\times(f_D+f_2)} = -\frac{1}{2}\varepsilon_2 R_e E_0^2 \sum_{n=-\infty}^{\infty} \sum_{m=-\infty}^{\infty} \\ \times \left(J_n(M_D) J_{n+1}(M_D) J_{m+1}(M_2) J_m(M_2) h_{(n+1,m+1)} h_{(n,m)} \sin\left(2\pi f_D t + \phi_{(n+1,m+1)} - \phi_{(n,m)}\right)\right) \tag{23}$$

Both of $V_{f_2\times(f_D-f_2)}$ and $V_{f_2\times(f_D+f_2)}$ will be demodulated using the reference signal $\sin(2\pi f_D t)$, and the demodulation output can be derived as

$$V_{error(f_D-f_2)} = \frac{1}{4}\varepsilon_2 R_e E_0^2 \sum_{n=-\infty}^{\infty} \sum_{m=-\infty}^{\infty} \\ \times \left(J_n(M_D) J_{n+1}(M_D) J_{m+1}(M_2) J_m(M_2) h_{(n+1,m)} h_{(n,m+1)} \cos\left(\phi_{(n+1,m)} - \phi_{(n,m+1)}\right)\right) \tag{24}$$

$$V_{error(f_D+f_2)} = -\frac{1}{4}\varepsilon_2 R_e E_0^2 \sum_{n=-\infty}^{\infty} \sum_{m=-\infty}^{\infty} \\ \times \left(J_n(M_D) J_{n+1}(M_D) J_{m+1}(M_2) J_m(M_2) h_{(n+1,m+1)} h_{(n,m)} \cos\left(\phi_{(n+1,m+1)} - \phi_{(n,m)}\right)\right) \tag{25}$$

When the total demodulation output $V_{error(f_D-f_2)} + V_{error(f_D+f_2)}$ is non-zero, the RIM leads to a non-zero output signal at the resonance center frequency. The output of synchronous demodulation is not only related to the amplitude, but also related to the phase. According to Eq. 20 and Eq. 21, Fig. 5(a) depicts the amplitude at frequency $f_D - f_2$ and $f_D + f_2$ on the PD1 as the frequency f_2 changes. It can be seen that the amplitude at frequency $f_D + f_2$ is greater than that at frequency $f_D - f_2$. Fig. 5(b) depicts the phase at frequency $f_D - f_2$ and $f_D + f_2$ on the PD1 as the frequency f_2 changes. It can be seen that the phase at frequency $f_D + f_2$ is different from that at frequency

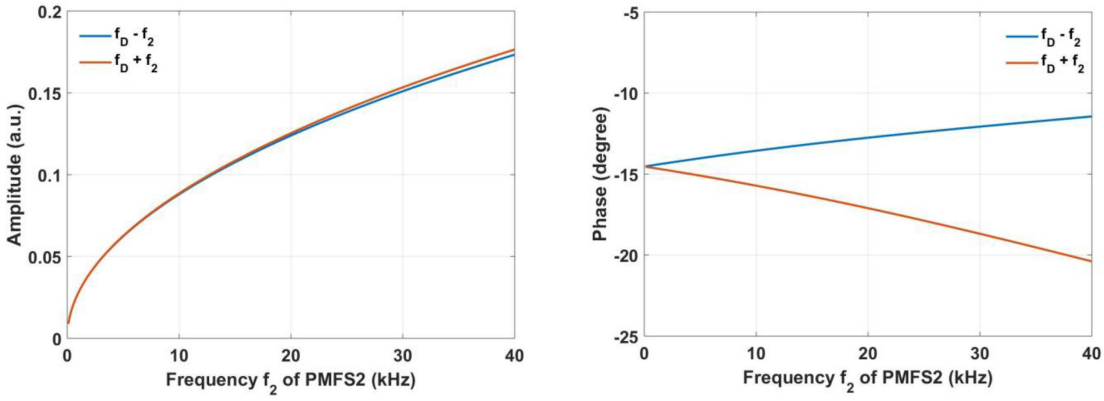

(a) Amplitude (b) Phase

Fig. 5. Amplitude and phase of the signal at frequency $f_D - f_2$ and $f_D + f_2$: $f_D = 160$kHz.

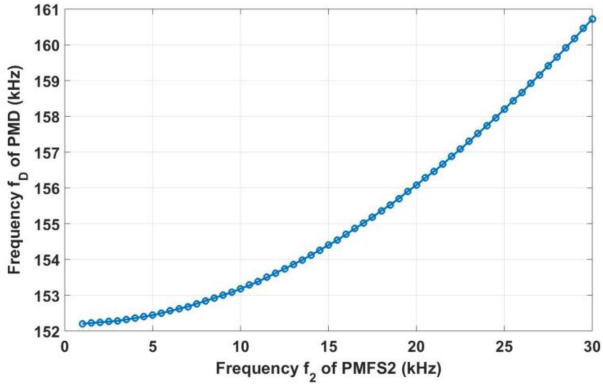

Fig. 6. Optimal combination of f_D and f_2.

$f_D - f_2$. According to Fig. 5, there are certain frequency combinations that make the total demodulation output $V_{error(f_D-f_2)} + V_{error(f_D+f_2)}$ zero. For example, when f_D and f_2 are 160kHz and 28.625kHz respectively, the amplitude at frequency $f_D - f_2$ and $f_D + f_2$ is approximately 0.1475 and 0.1498 respectively, and the phase is approximately -12.16° and -18.45° respectively. After calculation, the total demodulation output $V_{error(f_D-f_2)} + V_{error(f_D+f_2)}$ is zero, and the RIM will not induce a non-zero output signal at the resonance center frequency.

Therefore, there is an optimal combination of f_D and f_2 , which can effectively suppress the RIM-induced error. Fig. 6 shows the optimal combination of f_D and f_2. Under these combinations, the RIM-induced error is less than 0.01°/h. However, it should be pointed out that once the combination of f_D and f_2 deviates from these optimal combinations, the RIM-induced error will increase rapidly. Therefore, reducing the frequency of the PMFS may be a better method to suppress the error induced by the RIM of the PMFS.

3.3 Double Phase Modulation Technique

In the RFOG, both the RIM-induced error and the backscattering-induced noise need to be effectively suppressed. Compared to the RIM-induced error, the backscattering-induced noise is more serious, and theoretical analysis shows that the total carrier suppression of 120dB is required to reduce the backscattering-induced noise below the shot noise limited the sensitivity of the RFOG. The double phase modulation technique is proposed to further suppress the backscattering-induced noise [9]. The structure of the RFOG with the reciprocal detection and

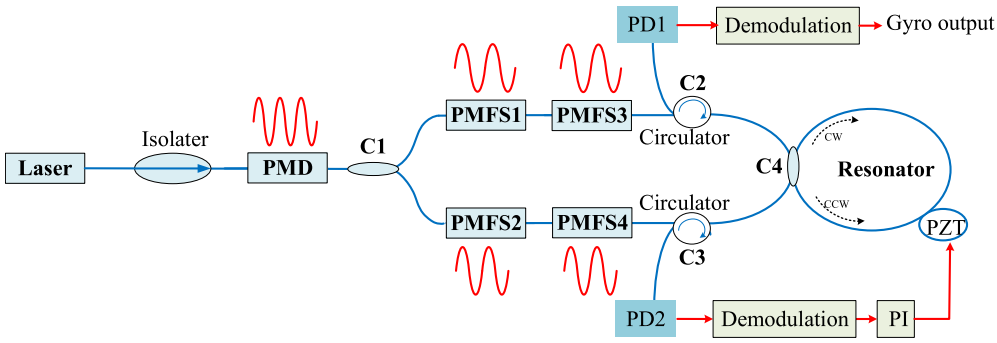

Fig. 7. Schematic diagram of the RFOG with the reciprocal detection and double phase modulation technique.

double phase modulation technique is shown in Fig. 7. Compared with Fig. 1, the phase modulators PMFS3 and PMFS4 are added to the CCW and CW circuits respectively to further suppress the backscattering-induced noise. Next, we analyze the error induced by the RIM of the added phase modulator. The modulation frequency and modulation index of the PMFS4 are f_4 and M_4, respectively. The RIM depth of the PMFS4 is ε_4.

The output field of the FRR can be rewritten as

$$E_{cw}(t)=\frac{\sqrt{2}}{2}E_0\left(1+\frac{1}{2}\varepsilon_2\sin(2\pi f_2 t)\right)\left(1+\frac{1}{2}\varepsilon_4\sin(2\pi f_4 t)\right)\times \sum_{n=-\infty}^{\infty}\sum_{m=-\infty}^{\infty}\sum_{q=-\infty}^{\infty}\left(J_n(M_D)J_m(M_2)J_q(M_4)\,e^{-i(2\pi f_S t+2\pi n f_D t+2\pi m f_2 t+2\pi q f_4 t)}h_{(n,m,q)}e^{i\phi_{(n,m,q)}}\right) \tag{26}$$

The output voltage of the PD1 can be rewritten as

$$V(t)=\frac{1}{2}R_e E_0^2\left(1+\varepsilon_2\sin(2\pi f_2 t)+\varepsilon_4\sin(2\pi f_4 t)\right)\times \sum_{n=-\infty}^{\infty}\sum_{n'=-\infty}^{\infty}\sum_{m=-\infty}^{\infty}\sum_{m'=-\infty}^{\infty}\sum_{q=-\infty}^{\infty}\sum_{q'=-\infty}^{\infty}\left(\begin{array}{l}J_n(M_D)J_{n'}(M_D)J_m(M_2)J_{m'}(M_2)J_q(M_4)J_{q'}(M_4)\times\\ e^{i(2\pi(n-n')f_D t+2\pi(m-m')f_2 t+2\pi(q-q')f_4 t)}h_{(n,m,q)}h_{(n',m',q')}e^{i\left(\phi_{(n,m,q)}-\phi_{(n',m',q')}\right)}\end{array}\right) \tag{27}$$

The voltage component at frequency f_D are demodulated by the LIA. The demodulated signal from the LIA can be expressed as

$$\begin{aligned}\Delta V(\Delta f)&=\frac{1}{2}R_e E_0^2\sum_{n=-\infty}^{\infty}\\ &\times\sum_{m=-\infty}^{\infty}\sum_{q=-\infty}^{\infty}\left(J_n(M_D)J_{n+1}(M_D)J_m^2(M_2)J_q^2(M_4)h_{(n,m,q)}h_{(n+1,m,q)}\sin\left(\phi_{(n+1,m,q)}-\phi_{(n,m,q)}\right)\right)\\ &-\frac{1}{4}\varepsilon_2 R_e E_0^2\sum_{n=-\infty}^{\infty}\sum_{m=-\infty}^{\infty}\sum_{q=-\infty}^{\infty}\left(\begin{array}{l}J_n(M_D)J_{n+1}(M_D)J_{m+1}(M_2)J_m(M_2)J_q^2(M_4)\times\\ \left(h_{(n+1,m+1,q)}h_{(n,m,q)}\cos\left(\phi_{(n+1,m+1,q)}-\phi_{(n,m,q)}\right)-h_{(n+1,m,q)}h_{(n,m+1,q)}\right.\\ \left.\cos\left(\phi_{(n+1,m,q)}-\phi_{(n,m+1,q)}\right)\right)\end{array}\right)\\ &-\frac{1}{4}\varepsilon_4 R_e E_0^2\sum_{n=-\infty}^{\infty}\sum_{m=-\infty}^{\infty}\sum_{q=-\infty}^{\infty}\left(\begin{array}{l}J_n(M_D)J_{n+1}(M_D)J_m^2(M_2)J_{q+1}(M_4)J_q(M_4)\times\\ \left(h_{(n+1,m,q+1)}h_{(n,m,q)}\cos\left(\phi_{(n+1,m,q+1)}-\phi_{(n,m,q)}\right)-h_{(n+1,m,q)}h_{(n,m,q+1)}\right.\\ \left.\cos\left(\phi_{(n+1,m,q)}-\phi_{(n,m,q+1)}\right)\right)\end{array}\right)\end{aligned} \tag{28}$$

Fig. 8 shows the relationship between f_2, f_4 and the RIM-induced error, where $f_D = 130$kHz and $\varepsilon_2 = \varepsilon_4 = 0.001$. It can be seen that reducing f_2 and f_4 can effectively suppress the RIM-induced error in the RFOG with reciprocal detection and double phase modulation technique. When f_2 and f_4 are 1kHz and 8kHz respectively, the RIM-induced error is calculated as 0.82°/h, which is higher than the sensitivity of the RFOG. However, when f_2 and f_4 are 1kHz and 2kHz respectively, the RIM-induced error is calculated as 0.06°/h, which is near the sensitivity of the RFOG. Therefore, when the phase modulator is added to the RFOG to further suppress the backscattering-induced

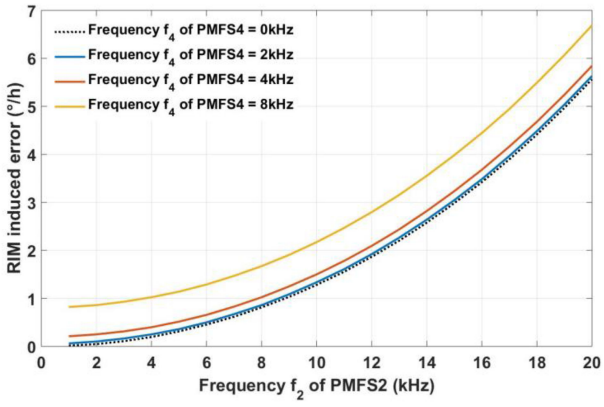

Fig. 8. Relationship between f_2, f_4 and RIM-induced error.

noise, the RIM-induced error can still be effectively suppressed by reducing the frequency of the added phase modulation.

4. Conclusion

In this paper, we established a model of the RIM-induced error in the RFOG with reciprocal detection, and the influences of the RIM of the PMFS on the performance of the RFOG are analyzed. The analysis shows that in order to reduce the bias to the level of the shot noise, it is necessary to suppress the error induced by the RIM of the PMFS, and reducing the RIM depth or reducing the modulation frequency of the PMFS can effectively suppress the RIM-induced error. There is an optimal combination of f_D and f_2, which can effectively suppress the RIM-induced error. When a phase modulator is added to the RFOG with reciprocal detection to further suppress the backscattering-induced noise, the RIM-induced error can still be effectively suppressed by reducing the frequency of the added phase modulation.

References

[1] H. C. Lefevre, *The Fiber-Optic Gyroscope*. Boston, MA, USA: Artech House, 2014.
[2] M. Smiciklas, G. Sanders, L. Strandjord, W. Williams, S. A. E. Benser, and F. Costin, "Development of a silicon photonics-based light source for compact resonator fiber optic gyroscopes," in *Proc. DGON Inertial Sensors Syst.*, 2019, pp. 1–12.
[3] G. Sanders, L. K. Strandjord, W. Williams, E. Benser, S. Ayotte, and F. Costin, "Improvements to signal processing and component minaturization of compact resonator fiber optic gyroscopes," in *Proc. DGON Inertial Sensors Syst.*, 2018, pp. 1–12.
[4] H. Li, Y. Lin, L. Liu, H. Ma, and Z. Jin, "Signal processing improvement of passive resonant fiber optic gyroscope using a reciprocal modulation-demodulation technique," *Opt. Exp.*, vol. 28, pp. 18103–18111, May 2020.
[5] Y. Zhang, L. Feng, H. Li, H. Jiao, N. Liu, and C. Zhang, "Resonant fiber optic gyroscope with three-frequency differential detection by sideband locking," *Opt. Exp.*, vol. 28, pp. 8423–8435, Mar. 2020.
[6] K. Shang, M. Lei, Y. Fang, H. Yu, and L. Zhang, "Resonator fiber-optic gyro with intensity error suppression using a bias-sampling compensation technique," *Appl. Opt.*, vol. 59, pp. 3995–3999, May 2020.
[7] X. Suo, H. Yu, J. Li, and X. Wu, "Transmissive resonant fiber-optic gyroscope employing kagome hollow-core photonic crystal fiber resonator," *Opt. Lett.*, vol. 45, pp. 2227–2230, Apr. 2020.
[8] H. Ma, J. Zhang, L. Wang, and Z. Jin, "Development and evaluation of optical passive resonant gyroscopes," *J. Lightw. Technol.*, vol. 35, pp. 3546–3554, Aug. 2017.
[9] H. Mao, H. Ma, and Z. Jin, "Polarization maintaining silica waveguide resonator optic gyro using double phase modulation technique," *Opt. Exp.*, vol. 19, pp. 4632–4643, Feb. 2011.
[10] H. Ma, Z. He, and K. Hotate, "Reduction of backscattering induced noise by carrier suppression in waveguide-type optical ring resonator gyro," *J. Lightw. Technol.*, vol. 29, no. 1, pp. 85–90, Jan. 2011.
[11] Z. Jiang, Z. Hu, W. Kang, J. Wang, and C. Fu, "Suppression of residual intensity modulation induced error in resonator fiber optic gyroscopes with improved modulation technique," *Opt. Commun.*, vol. 459, Mar. 2020, Art. no. 124936.
[12] N. Liu, Y. Niu, L. Feng, H. Jiao, and X. Wang, "Suppression of backscattering induced noise by the sideband locking technique in a resonant fiber optic gyroscope," *Chin. Opt. Lett.*, vol. 16, Sep. 2018, Art. no. 010608.

[13] J. Wang, L. Feng, Q. Wang, H. Jiao, and X. Wang, "Suppression of backreflection error in resonator integrated optic gyro by the phase difference traversal method," *Opt. Lett.*, vol. 41, pp. 1586–1589, Apr. 2016.
[14] Z. Jiang, Z. Hu, W. Kang, J. Wang, and C. Fu, "Residual intensity modulation-induced error in resonator fiber optic gyroscopes with triangular phase modulation," *Appl. Opt.*, vol. 58, pp. 7597–7602, Sep. 2019.
[15] D. Ying, Q. Li, H. Ma, and Z. Jin, "Residual intensity modulation in resonator fiber optic gyros with sinusoidal wave phase modulation," *J. Zhejiang Univ.-Sci. C (Comput. Electron.)*, vol. 15, pp. 482–488, Jul. 2014.
[16] C. Zhang, Z. Pan, Y. Zheng, P. An, J. Tang, and J. Liu. "Suppression of residual intensity modulation noise in resonator integrated optic gyro," *Opt. Commun.*, vol. 430, pp. 358–363, Jan. 2019.
[17] J. Sathian and, and E. Jaatinen, "Intensity dependent residual amplitude modulation in electro-optic phase modulators," *Appl. Opt.*, vol. 51, pp. 3684–3691, Jun. 2012.
[18] C. Antao, and J. M. Edmond. *Broadband Optical Modulations*. Boca Raton, FL, USA: CRC Press, 2011.